Approximate Osher-Solomon schemes for hyperbolic systems

Manuel J. Castro[1], José M. Gallardo[1,*], Antonio Marquina[b]

[a] *Departamento de Análisis Matemático, Universidad de Málaga, Campus de Teatinos s/n, Málaga 29080, Spain*
[b] *Departamento de Matemática Aplicada, Universidad de Valencia, Avda. Dr. Moliner 50, Burjassot-Valencia 46100, Spain*

Abstract

This paper is concerned with a new kind of Riemann solvers for hyperbolic systems, which can be applied both in the conservative and nonconservative cases. In particular, the proposed schemes constitute a simple version of the classical Osher-Solomon Riemann solver, and extend in some sense the schemes proposed in [19, 20]. The viscosity matrix of the numerical flux is constructed as a linear combination of functional evaluations of the Jacobian of the flux at several quadrature points. Some families of functions have been proposed to this end: Chebyshev polynomials and rational-type functions. Our schemes have been tested with different initial value Riemann problems for ideal gas dynamics, magnetohydrodynamics and multilayer shallow water equations. The numerical tests indicate that the proposed schemes are robust, stable and accurate with a satisfactory time step restriction, and provide an efficient alternative for approximating time-dependent solutions in which the spectral decomposition is computationally expensive.

Keywords: Hyperbolic systems, nonconservative products, incomplete Riemann solvers, Osher-Solomon method, Euler equations, ideal magnetohydrodynamics, multilayer shallow water equations

[☆]This research has been partially supported by the Spanish Government Research projects MTM2012-38383 and MTM2011-28043. The numerical computations have been performed at the Laboratory of Numerical Methods of the University of Málaga.

[*]Corresponding author

Email addresses: castro@anamat.cie.uma.es (Manuel J. Castro), jmgallardo@uma.es (José M. Gallardo), marquina@uv.es (Antonio Marquina)

1. Introduction

The Osher-Solomon scheme ([31]) is a nonlinear and complete Riemann solver which enjoys a number of attractive features: it is robust, entropy-satisfying, smooth (i.e., differentiable with respect to its arguments) and has a good behavior when computing slowly-moving shocks. However, it requires the computation of a path-dependent integral in phase space, which makes it very complex and computationally expensive. Due to this difficulties, its practical application has been restricted to certain systems, e.g., the compressible Euler equations ([36]).

In [19, 20], the authors proposed a new version of the Osher-Solomon method in which the integrals in phase space are numerically approximated by means of a Gauss-Legendre quadrature formula. This leads to a scheme much simpler than the original one, which is also applicable to general hyperbolic systems. In particular, the viscosity matrix of the numerical flux is defined as a linear combination of the absolute value matrix of the physical flux evaluated at certain quadrature points. The computation of these absolute value matrices requires the knowledge of the complete eigenstructure of the system. Thus, for systems in which the eigenstructure is not known or difficult to compute, the scheme may be computationally expensive.

In this paper we propose an alternative version of the universal Osher-Solomon scheme in [19, 20], in which the absolute value matrices are approximated by means of appropriate functional evaluations of the Jacobian of the flux evaluated at the quadrature points. The only information these schemes require is a bound on the maximum speed of propagation. Several families of approximations have been considered. The first one is based on Chebyshev polynomials, which provide optimal uniform approximations to the absolute value function. As an additional feature, the associated Osher-Solomon schemes admit a free-Jacobian implementation. On the other hand, it is well-known that the order of approximation to $|x|$ can be greatly improved by using rational functions instead of polynomials. For this reason, two different families of rational approximations have also been considered, based on Newman ([29]) and Halley ([7]) functions. This families of functions have also been considered in the recently introduced RVM schemes (see [12]).

It should be noticed that the proposed approximate Osher-Solomon schemes can be defined for general conservative and nonconservative systems. Moreover, they can also be extended to high-order and multidimensions, following the guidelines in [10, 13]. In the conservative case, the schemes have been applied to a number of initial value Riemann problems

for ideal gas dynamics and magnetohydrodynamics, to observe their behavior with respect to some challenging scenarios in numerical simulations. On the other hand, the two-layer shallow water equations have been considered to test the schemes in the nonconservative framework, as they constitute a representative example including both source and nonconservative coupling terms. Our numerical tests indicate that the proposed schemes are robust, running stable and accurate with a satisfactory time step restriction. Comparisons with the Osher-Solomon and some other well-known schemes in the literature (e.g., Roe and HLL) have also been performed.

The paper is organized as follows. In Section 2 we give some basic concepts needed to review, in Section 3, the classical Osher-Solomon scheme and its extension proposed by Dumbser and Toro in [19, 20]. The proposed approximate Osher-Solomon schemes for conservative hyperbolic systems are then introduced in Section 4. The extension to the nonconservative framework is done in Section 5. Several applications to the Euler and ideal magnetohydrodynamics equations are presented in Section 6, while Section 7 is devoted to the two-layer shallow water equations. Some conclusions are drawn in Section 8. Finally, Appendix A contains some details about the implementation of the approximate Osher-Solomon schemes based on Chebyshev approximations, including its free-Jacobian version.

2. Preliminaries

Consider a hyperbolic system of conservation laws

$$\partial_t w + \partial_x F(w) = 0, \tag{1}$$

where $w(x,t)$ takes values on an open convex set $\mathcal{O} \subset \mathbb{R}^N$ and $F\colon \mathcal{O} \to \mathbb{R}^N$ is a smooth flux function. We are interested in the numerical solution of the Cauchy problem for (1) by means of finite volume methods of the form

$$w_i^{n+1} = w_i^n - \frac{\Delta t}{\Delta x}(F_{i+1/2} - F_{i-1/2}), \tag{2}$$

where w_i^n denotes the approximation to the average of the exact solution at the cell $I_i = [x_{i-1/2}, x_{i+1/2}]$ at time $t^n = n\Delta t$ (the dependence on time will be dropped unless necessary). We assume that the numerical flux is given by

$$F_{i+1/2} = \frac{F(w_i) + F(w_{i+1})}{2} - \frac{1}{2} Q_{i+1/2}(w_{i+1} - w_i), \tag{3}$$

where $Q_{i+1/2}$ denotes the numerical *viscosity matrix*, which determines the numerical diffusion of the scheme.

The condition of hyperbolicity of system (1) states that the Jacobian matrix of the flux at each state $w \in \mathcal{O}$,

$$A(w) = \frac{\partial F}{\partial w}(w),$$

can be diagonalized as

$$A = PDP^{-1},$$

where $D = \mathrm{diag}(\lambda_1, \ldots, \lambda_N)$, λ_i being the eigenvalues of A, and the matrix P is composed by the associated right eigenvalues of A. As it is usual, we denote the positive and negative parts of A, respectively, as

$$A^+ = PD^+P^{-1}, \quad A^- = PD^-P^{-1},$$

where $D^\pm = \mathrm{diag}(\lambda_1^\pm, \ldots, \lambda_N^\pm)$, with $\lambda_i^+ = \max(\lambda_i, 0)$ and $\lambda_i^- = \min(\lambda_i, 0)$. It is clear that $A = A^+ + A^-$. On the other hand, the absolute value of A is defined as

$$|A| = A^+ - A^-.$$

It is interesting to note that Roe's method ([35]) can be written in the form (3) with viscosity matrix given by $Q_{i+1/2} = |A_{i+1/2}|$, where $A_{i+1/2}$ is a Roe matrix for the system. Several numerical methods have been developed by using approximations to $|A_{i+1/2}|$ as viscosity matrices; see, e.g., [15, 17, 23, 36, 37] and the references therein. A general approach to build such kind of approximations by means of polynomial or rational functions has recently been introduced in [9] and [12]. In particular, it has been shown that a number of well-known schemes in the literature can be viewed as particular cases within this general approach: Roe, Lax-Friedrichs, Rusanov, HLL, FORCE, etc.

3. The Osher-Solomon scheme

The Osher-Solomon scheme ([31]) is a nonlinear Riemann solver that possesses a number of interesting features: it is entropy-satisfying, robust, differentiable and good behaved for slowly-moving shocks. On the contrary, its implementation is rather cumbersome, computationally expensive, and only applicable to certain systems.

Let $A(w)$ be the Jacobian of F evaluated at w, and assume the flux splitting

$$F(w) = F^+(w) + F^-(w), \tag{4}$$

where

$$A^{\pm}(w) = \frac{\partial F^{\pm}}{\partial w}(w).$$

The *classical Osher-Solomon numerical flux* is then defined as

$$F_{i+1/2} = F^{+}(w_i) + F^{-}(w_{i+1}).$$

Let now Φ be a path in the phase-space $\mathcal{O}$ linking the states w_i and w_{i+1}, i.e., $\Phi\colon [0,1] \to \mathcal{O}$ is a Lipschitz continuous function such that $\Phi(0) = w_i$ and $\Phi(1) = w_{i+1}$. Then, we can write

$$F^{-}(w_{i+1}) - F^{-}(w_i) = \int_0^1 A^{-}(\Phi(s))\Phi'(s)ds,$$

from which we deduce

$$F_{i+1/2} = F(w_i) + \int_0^1 A^{-}(\Phi(s))\Phi'(s)ds. \tag{5}$$

Similarly, we could also write

$$F_{i+1/2} = F(w_{i+1}) - \int_0^1 A^{+}(\Phi(s))\Phi'(s)ds. \tag{6}$$

Combining (5) and (6), the Osher-Solomon flux can be written as

$$F_{i+1/2} = \frac{F(w_i) + F(w_{i+1})}{2} - \frac{1}{2}\int_0^1 \big|A(\Phi(s))\big|\Phi'(s)ds. \tag{7}$$

Notice that the flux splitting (4) is not explicitely needed in formula (7).

The expression (7) for the numerical flux depends on the path Φ in phase-space, so in general it may be difficult to compute. Osher and Solomon ([31]) proposed a way to build, under certain assumptions, a path which makes possible to perform the integration. Unfortunately, the resulting solver is rather complex, computationally expensive, and only applicable to certain systems (see [36] for an application to the compressible Euler equations).

Following [19], a way to circumvent the drawbacks of the Osher-Solomon solver, maintaining at the same time its good features, is explained in what follows. First, the simple path consisting in segments is chosen, that is,

$$\Phi(s) = w_i + s(w_{i+1} - w_i), \quad s \in [0,1].$$

Thus (7) can be written as

$$F_{i+1/2} = \frac{F(w_i) + F(w_{i+1})}{2} - \frac{1}{2}\left(\int_0^1 \big|A(w_i + s(w_{i+1} - w_i))\big| ds \right)(w_{i+1} - w_i). \tag{8}$$

Comparing (7) with (3), the viscosity matrix of the scheme is, in this case,

$$Q_{i+1/2} = \int_0^1 \big|A(w_i + s(w_{i+1} - w_i))\big| ds.$$

To avoid the analytical integration, which may be difficult, the integral can be evaluated numerically using a Gauss-Legendre quadrature formula. In this case, the Osher-Solomon flux has the following form:

$$F_{i+1/2} = \frac{F(w_i) + F(w_{i+1})}{2} - \frac{1}{2}\left(\sum_{k=1}^{q} \omega_k \big|A(w_i + s_k(w_{i+1} - w_i))\big| \right)(w_{i+1} - w_i), \tag{9}$$

where $s_k \in [0, 1]$ and ω_k are the weights of the quadrature formula. The resulting scheme is simple to implement and applicable to general hyperbolic systems. On the other hand, it needs the full eigenstructure of the system, which can be computed numerically when it is not known or difficult to calculate.

4. Approximate Osher-Solomon schemes

With the aim of simplifying the computation of the numerical flux (9), it would be desiderable to approximate the intermediate matrices

$$\big|A(w_i + s_k(w_{i+1} - w_i))\big|, \quad k = 1, \ldots, q,$$

in a simple and efficient way. Two approaches will be considered in this section, one based on Chebyshev polynomials and another relying on rational approximations.

Let $P(x)$ be a polynomial approximation to the absolute value function $|x|$ in the interval $[-1, 1]$, satisfying the *stability condition* ([9])

$$|x| \leq P(x) \leq 1, \quad \forall\, x \in [-1, 1]. \tag{10}$$

For a given matrix A, if $\lambda_{\max}$ is the eigenvalue of A with maximum absolute value (or an upper bound of it), $|A|$ can be approximated as

$$|A| \approx |\lambda_{\max}| P\big(|\lambda_{\max}|^{-1} A\big).$$

Denote

$$A^{(k)}_{i+1/2} = A(w_i + s_k(w_{i+1} - w_i)), \quad k = 1, \ldots, q,$$

where A is the Jacobian matrix of F, and let $\lambda^{(k)}_{i+1/2,\max}$ be the eigenvalue of $A^{(k)}_{i+1/2}$ with maximum absolute value. Then, the *polynomial approximate Osher-Solomon* flux is defined as

$$F_{i+1/2} = \frac{F(w_i) + F(w_{i+1})}{2} - \frac{1}{2}\left(\sum_{k=1}^{q} \omega_k \widetilde{P}^{(k)}_{i+1/2}\right)(w_{i+1} - w_i), \tag{11}$$

where

$$\widetilde{P}^{(k)}_{i+1/2} = |\lambda^{(k)}_{i+1/2,\max}| P\left(|\lambda^{(k)}_{i+1/2,\max}|^{-1} A^{(k)}_{i+1/2}\right). \tag{12}$$

In this case, the viscosity matrix is given by $Q_{i+1/2} = \sum_{k=1}^{q} \omega_k \widetilde{P}^{(k)}_{i+1/2}$.

Remark 1. The advantage of formula (11) with respect to (9) is that in the latter it is necessary to compute the full eigenstructure of the system, while in the former only an upper bound on the spectral radius is needed. □

Notice that the closer the polynomial $P(x)$ is to $|x|$ in the uniform norm, the more similar the approximate flux (11) will be to the Osher-Solomon flux (9). This suggests to use accurate polynomial approximations to $|x|$ for building (11). In particular, Chebyshev approximations will be considered in the numerical experiments. Specifically, for a given $p \geq 1$ we take $P(x) = \tau_{2p}(x)$, where

$$\tau_{2p}(x) = \frac{2}{\pi} + \frac{4}{\pi} \sum_{j=1}^{p} \frac{(-1)^{j+1}}{(2j-1)(2j+1)} T_{2j}(x), \quad x \in [-1, 1], \tag{13}$$

and the Chebyshev polynomials of even degree $T_{2j}(x)$ are recursively defined as

$$T_0(x) = 1, \quad T_2(x) = 2x^2 - 1, \quad T_{2j}(x) = 2T_2(x)T_{2j-2}(x) - T_{2j-4}(x). \tag{14}$$

Following [2], the order of approximation of $\tau_{2p}(x)$ to $|x|$ is optimal in the $L^\infty(-1, 1)$ norm. Moreover, the recursive definition of the polynomials $T_{2k}(x)$ provides an explicit and efficient way to compute $\tau_{2p}(x)$.

It is worth noting that the implementation of the approximate Osher-Solomon scheme with Chebyshev polynomials does not require the computation of the matrices $\widetilde{P}^{(k)}_{i+1/2}$, but only of the vectors $\widetilde{P}^{(k)}_{i+1/2}(w_{i+1} - w_i)$.

Futhermore, the recursive form of the Chebyshev polynomials allows to construct a Jacobian-free implementation of the approximate Osher-Solomon scheme. The details can be found in Appendix A.

As it is well-known, the order of approximation to $|x|$ can be greatly improved by using rational functions instead of polynomials. This suggests to consider *rational approximate Osher-Solomon* fluxes of the form

$$F_{i+1/2} = \frac{F(w_i) + F(w_{i+1})}{2} - \frac{1}{2}\left(\sum_{k=1}^{q} \omega_k \widetilde{R}^{(k)}_{i+1/2}\right)(w_{i+1} - w_i), \tag{15}$$

where $\widetilde{R}^{(k)}_{i+1/2}$ is defined as in (12), but taking as basis function a rational approximation $R(x)$ to $|x|$ satisfying the stability condition (10). Following [12], two different families of rational functions will be considered:

- Given a set of $r \geq 4$ distinct points $X = \{0 < x_1 < \cdots < x_r \leq 1\}$, construct the polynomial

$$p(x) = \prod_{k=1}^{r} (x + x_k).$$

  The *Newman rational function* ([29]) associated to X is defined as

$$R_r(x) = x\,\frac{p(x) - p(-x)}{p(x) + p(-x)}.$$

  The rate of approximation of $R_r(x)$ to $|x|$ depends on the choice of nodes X: several possibilities can be found in the literature [5, 6, 29]. Here, we will take $x_k = \exp(-kr^{-1/2})$, which provides an exponential rate of approximation ([29]).

- The *Halley rational functions* $H_r(x)$ are recursively defined as ([12])

$$H_{r+1}(x) = H_r(x)\,\frac{H_r(x)^2 + 3x^2}{3H_r(x)^2 + x^2}, \quad H_0(x) = 1.$$

  It can be proved ([7]) that $\|H_r(x) - |x|\|_\infty = 3^{-r}$.

Both the Chebyshev polynomials $\tau_{2p}(x)$ and the Newman functions $R_r(x)$ do not satisfy the stability condition (10) strictly, although this can be easily fixed with a slight modification: see [12] for details. However, in practical computations there are no appreciable differences between both approaches. On the other hand, Halley functions $H_r(x)$ satisfy (10) by construction. As long as the functions considered do not cross the origin, no entropy-fix is needed in the presence of sonic points.

5. Extension to the nonconservative case

The approximate Osher-Solomon schemes introduced in the previous sections can be extended to the case of nonconservative hyperbolic systems, of the form

$$\partial_t W + \mathcal{A}(W)\partial_x W = 0. \tag{16}$$

Here the matrix $\mathcal{A}(W)$ is assumed to be strictly hyperbolic for each state W belonging to an open convex subset $\Omega \subset \mathbb{R}^M$. The theoretical issues concerning the definition of weak solutions for (16) can be found in [27], and will not be treated here. However, it is important to remark that the definition of the nonconservative product $\mathcal{A}(W)\partial_x W$ relies on the choice of a family of paths Φ linking arbitrary states in the phase space Ω.

Numerical approximations to the solutions of (16) can be obtained by means of *path-conservative* finite volume schemes of the form (see [32] for details):

$$W_i^{n+1} = W_i^n - \frac{\Delta t}{\Delta x}(\mathcal{D}^+_{i-1/2} + \mathcal{D}^-_{i+1/2}), \tag{17}$$

where $\mathcal{D}^\pm_{i+1/2} = \mathcal{D}^\pm(W_i^n, W_{i+1}^n)$, $\mathcal{D}^-$ and $\mathcal{D}^+$ being two continuous functions from Ω^2 to Ω satisfying

$$\mathcal{D}^\pm(W, W) = 0, \quad \forall\, W \in \Omega,$$

and

$$\mathcal{D}^-(W_0, W_1) + \mathcal{D}^+(W_0, W_1) = \int_0^1 \mathcal{A}(\Phi(s; W_0, W_1))\frac{\partial \Phi}{\partial s}(s; W_0, W_1)\, ds \tag{18}$$

for every $W_0, W_1 \in \Omega$. In particular, the *generalized Roe's scheme* ([33]) can be defined by

$$\mathcal{D}^\pm_{i+1/2} = \frac{1}{2}\big(\mathcal{A}_\Phi(W_i^n, W_{i+1}^n) \pm |\mathcal{A}_\Phi(W_i^n, W_{i+1}^n)|\big)(W_{i+1}^n - W_i^n),$$

where $\mathcal{A}_\Phi$ is a *Roe linearization* ([39]) associated to $\mathcal{A}$ and Φ. In this case, the term $|\mathcal{A}_\Phi(W_i^n, W_{i+1}^n)|$ may be interpreted as the viscosity matrix of the numerical flux. Using Roe's property, it is possible to write Roe's fluxes as

$$\mathcal{D}^\pm_{i+1/2} = \frac{1}{2}\int_0^1 \mathcal{A}(\Phi(s; W_i^n, W_{i+1}^n))\frac{\partial \Phi}{\partial s}(s; W_i^n, W_{i+1}^n)\, ds \pm \frac{1}{2}|\mathcal{A}_\Phi(W_i^n, W_{i+1}^n)|(W_{i+1}^n - W_i^n).$$

It is then natural to define the *generalized Osher-Solomon* fluxes as follows:

$$\mathcal{D}^{\pm}_{i+1/2} = \frac{1}{2}\int_0^1 \mathcal{A}(\Phi(s;W_i^n,W_{i+1}^n))\frac{\partial\Phi}{\partial s}(s;W_i^n,W_{i+1}^n)\,ds \\ \pm \frac{1}{2}\int_0^1 |\mathcal{A}(\Phi(s;W_i^n,W_{i+1}^n))|\frac{\partial\Phi}{\partial s}(s;W_i^n,W_{i+1}^n)\,ds, \quad (19)$$

or, equivalently,

$$\mathcal{D}^{\pm}_{i+1/2} = \frac{1}{2}\mathcal{A}_\Phi(W_i^n,W_{i+1}^n)(W_{i+1}^n - W_i^n) \\ \pm \frac{1}{2}\int_0^1 |\mathcal{A}(\Phi(s;W_i^n,W_{i+1}^n))|\frac{\partial\Phi}{\partial s}(s;W_i^n,W_{i+1}^n)\,ds, \quad (20)$$

The above expressions can be viewed as generalizations of the Osher-Solomon flux formula (7) to the nonconservative framework. A similar approach has also been considered in [20].

Remark 2. It is worth noting that the equivalence between (19) and (20) relies on the existence of the Roe linearization $\mathcal{A}_\Phi$. In this sense, formula (19) is more general and could be used in those cases in which a Roe linearization is not known or difficult to compute. □

As it was pointed out in [32], the proper choice of the family of paths Φ may be difficult or very costly in practice, and usually relies on the physics of the problem under consideration. For these reasons, it is common in the literature to consider the simpler family of segments: $\Phi(s;W_L,W_R) = W_L + s(W_R - W_L)$, and this choice will be assumed throughout the rest of the paper. Doing so, and denoting $\mathcal{A}_{i+1/2} = \mathcal{A}_\Phi(W_i^n, W_{i+1}^n)$ for the sake of simplicity, the Osher-Solomon fluxes have the following form:

$$\mathcal{D}^{\pm}_{i+1/2} = \frac{1}{2}\left(\mathcal{A}_{i+1/2} \pm \int_0^1 |\mathcal{A}(W_i^n + s(W_{i+1}^n - W_i^n))|\,ds\right)(W_{i+1}^n - W_i^n),$$

which constitutes an extension of formula (8) to the nonconservative setting. In particular, the integral $\int_0^1 |\mathcal{A}(W_i^n + s(W_{i+1}^n - W_i^n))|\,ds$ can be interpreted as the viscosity term of the numerical flux. Reasoning as in Section 3, this integral can be approximated by means of a Gauss-Legendre quadrature formula, which leads to

$$\mathcal{D}^{\pm}_{i+1/2} = \frac{1}{2}\left(\mathcal{A}_{i+1/2} \pm \sum_{k=1}^{q}\omega_k|\mathcal{A}^{(k)}_{i+1/2}|\right)(W_{i+1}^n - W_i^n), \quad (21)$$

where $\mathcal{A}^{(k)}_{i+1/2} = \mathcal{A}(W^n_i + s_k(W^n_{i+1} - W^n_i))$, using a similar notation as in Section 4.

Remark 3. It is also reasonable to apply the quadrature formula directly to (19), in which case the corresponding flux has the form

$$\mathcal{D}^{\pm}_{i+1/2} = \frac{1}{2}\left(\sum_{k=1}^{q} \omega_k \big(\mathcal{A}^{(k)}_{i+1/2} \pm |\mathcal{A}^{(k)}_{i+1/2}|\big)\right)(W^n_{i+1} - W^n_i). \tag{22}$$

Notice that this formula does not depend explicitely on any Roe linearization $\mathcal{A}_\Phi$ (see Remark 2). On the contrary, the resulting scheme is not strictly path-conservative, as condition (18) only holds approximately. □

Once formula (21) has been derived, approximate Osher-Solomon schemes for the nonconservative system (16) can be constructed in a natural way, following the guidelines in Section 4. Specifically, the numerical fluxes for a *polynomial Osher-Solomon scheme* will have the form

$$\mathcal{D}^{\pm}_{i+1/2} = \frac{1}{2}\left(\mathcal{A}_{i+1/2} \pm \sum_{k=1}^{q} \omega_k \widetilde{P}^{(k)}_{i+1/2}\right)(W^n_{i+1} - W^n_i),$$

where $P(x)$ is a polynomial approximation to $|x|$ satisfying the stability condition (10), and $\widetilde{P}^{(k)}_{i+1/2}$ is defined in (12). In a similar way, *rational Osher-Solomon schemes* are obtained when the polynomial $P(x)$ is substituted by a rational function $R(x)$.

Consider now the particular case of a hyperbolic system of conservation laws with source terms and nonconservative products, that is,

$$\partial_t w + \partial_x F(w) + B(w)\partial_x w = G(w)\partial_x H, \tag{23}$$

where $w(x,t) \in \mathcal{O}$ ($\mathcal{O}$ being an open convex subset of $\mathbb{R}^N$), $F\colon \mathcal{O} \to \mathbb{R}^N$ is a smooth flux function, $B\colon \mathcal{O} \to \mathcal{M}_N(\mathbb{R})$ is a smooth matricial function, and $G\colon \mathcal{O} \to \mathbb{R}^N$ and $H\colon \mathbb{R} \to \mathbb{R}$ are given functions. System (23) can be written in the form (16) considering the trivial equation $\partial_t H = 0$ and defining

$$W = \begin{pmatrix} w \\ H \end{pmatrix} \in \Omega = \mathcal{O} \times \mathbb{R} \subset \mathbb{R}^{N+1}, \quad \mathcal{A}(W) = \begin{pmatrix} A(w) & -G(w) \\ 0 & 0 \end{pmatrix},$$

where $A(w) = \frac{\partial F}{\partial w}(w) + B(w)$. In this case, a Roe linearization $\mathcal{A}_{i+1/2}$ can be built as ([33])

$$\mathcal{A}_{i+1/2} = \begin{pmatrix} A_{i+1/2} & -G_{i+1/2} \\ 0 & 0 \end{pmatrix},$$

where $A_{i+1/2} = \mathcal{L}_{i+1/2} + B_{i+1/2}$, $\mathcal{L}_{i+1/2}$ being a Roe matrix for the flux F in the usual sense, that is, $\mathcal{L}_{i+1/2}(w_{i+1}^n - w_i^n) = F(w_{i+1}^n) - F(w_i^n)$; $B_{i+1/2}$ is a matrix verifying

$$B_{i+1/2}(w_{i+1}^n - w_i^n) = \left(\int_0^1 B(w_i^n + s(w_{i+1}^n - w_i^n))\, ds \right)(w_{i+1}^n - w_i^n),$$

while $G_{i+1/2}$ is a vector that satisfies

$$G_{i+1/2}(H_{i+1} - H_i) = \left(\int_0^1 G(w_i^n + s(w_{i+1}^n - w_i^n))\, ds \right)(H_{i+1} - H_i).$$

Assuming that $A(w)$ is nonsingular, it is straightforward to check that

$$|\mathcal{A}(W)| = \begin{pmatrix} |A(w)| & -|A(w)|A(w)^{-1}G(w) \\ 0 & 0 \end{pmatrix}.$$

This allows to develop (21) and express $\mathcal{D}_{i+1/2}^{\pm}$ in terms of $A_{i+1/2}$, $B_{i+1/2}$ and $G_{i+1/2}$. After this process, and coming back to the original variable w, the Osher-Solomon scheme for solving (23) can be written as

$$w_{i+1}^n = w_i^n - \frac{\Delta t}{\Delta x}(D_{i-1/2}^+ + D_{i+1/2}^-), \tag{24}$$

with numerical fluxes given by

$$D_{i+1/2}^{\pm} = \frac{1}{2}\Bigg(F(w_{i+1}^n) - F(w_i^n) + B_{i+1/2}(w_{i+1}^n - w_i^n) - G_{i+1/2}(H_{i+1} - H_i) \\ \pm \sum_{k=1}^{q} \omega_k |A_{i+1/2}^{(k)}| \big(w_{i+1}^n - w_i^n - (A_{i+1/2}^{(k)})^{-1} G_{i+1/2}^{(k)}(H_{i+1} - H_i) \big) \Bigg), \tag{25}$$

where $A_{i+1/2}^{(k)} = A(w_i^n + s_k(w_{i+1}^n - w_i^n))$, and similarly for $G_{i+1/2}^{(k)}$.

Finally, approximate polynomial Osher-Solomon schemes for (23) are obtained when the matrices $|A_{i+1/2}^{(k)}|$ in (25) are substituted by $\widetilde{P}_{i+1/2}^{(k)}$. The resulting fluxes read

$$D_{i+1/2}^{\pm} = \frac{1}{2}\Bigg(F(w_{i+1}^n) - F(w_i^n) + B_{i+1/2}(w_{i+1}^n - w_i^n) - G_{i+1/2}(H_{i+1} - H_i) \\ \pm \sum_{k=1}^{q} \omega_k \widetilde{P}_{i+1/2}^{(k)} \big(w_{i+1}^n - w_i^n - (A_{i+1/2}^{(k)})^{-1} G_{i+1/2}^{(k)}(H_{i+1} - H_i) \big) \Bigg). \tag{26}$$

In a similar way, approximate rational Osher-Solomon schemes are defined by changing $\widetilde{P}_{i+1/2}^{(k)}$ by $\widetilde{R}_{i+1/2}^{(k)}$ in (26).

Remark 4. For a system of conservation laws (that is, $B = 0$ and $G = 0$), the scheme (24) can be written in the form (2) by simply taking $F_{i+1/2} = D^-_{i+1/2} + F(w^n_i)$ or, equivalently, $F_{i+1/2} = -D^+_{i+1/2} + F(w^n_{i+1})$, which in turn coincides with formula (9). □

6. Applications to the Euler and ideal magnetohydrodynamics equations

This section is devoted to test the performances of the approximate Osher-Solomon schemes introduced in the previous sections. In particular, we will consider to some challenging problems related to the Euler and ideal magnetohydrodynamics equations.

The ideal magnetohydrodynamics (MHD) system of equations has the following form:

$$\begin{cases} \partial_t \rho = -\nabla \cdot (\rho \mathbf{v}), \\ \partial_t (\rho \mathbf{v}) = -\nabla \cdot \left(\rho \mathbf{v}\mathbf{v}^T + \left(P + \frac{1}{2}\mathbf{B}^2 \right) I - \mathbf{B}\mathbf{B}^T \right), \\ \partial_t \mathbf{B} = \nabla \times (\mathbf{v} \times \mathbf{B}), \\ \partial_t E = -\nabla \cdot \left(\left(\frac{\gamma}{\gamma - 1} P + \frac{1}{2}\rho q^2 \right) \mathbf{v} - (\mathbf{v} \times \mathbf{B}) \times \mathbf{B} \right), \end{cases} \tag{27}$$

where ρ represents the mass density, $\mathbf{v} = (v_x, v_y, v_z)^t$ and $\mathbf{B} = (B_x, B_y, B_z)^t$ are the velocity and magnetic fields, and E is the total energy. If q and B denote the magnitudes of the velocity and magnetic fields, the total energy can be expressed as

$$E = \frac{1}{2}\rho q^2 + \frac{1}{2}B^2 + \rho\varepsilon,$$

where the specific internal energy ε is related to the hydrostatic pressure P through the equation of state $P = (\gamma - 1)\rho\varepsilon$, γ being the adiabatic constant. The total pressure P^* is then defined as $P + P_M$, where $P_M = \frac{1}{2}B^2$ is the magnetic pressure. In addition to the equations, the magnetic field satisfies the divergence-free condition

$$\nabla \cdot \mathbf{B} = 0. \tag{28}$$

Notice that if $\mathbf{B} = \mathbf{0}$ then system (27) reduces to the Euler equations for ideal gases.

Let us define $(b_x, b_y, b_z) = (B_x, B_y, B_z)/\sqrt{\rho}$, $b^2 = b_x^2 + b_y^2 + b_z^2$, and the acoustic sound speed $a = \sqrt{\gamma P/\rho}$. The Alfven, fast and slow waves are, respectively,

$$c_a = |b_x|, \quad c_{f,s}^2 = \frac{1}{2}\big(a^2 + b^2 \pm \sqrt{(a^2+b^2)^2 - 4a^2 b_x^2}\big).$$

The eight characteristic velocities are then given by

$$\begin{aligned} &\lambda_1 = u - c_f, \quad \lambda_2 = u - c_a, \quad \lambda_3 = u - c_s, \quad \lambda_4 = u, \\ &\lambda_5 = u, \quad \lambda_6 = u + c_s, \quad \lambda_7 = u + c_a, \quad \lambda_8 = u + c_f. \end{aligned}$$

The characteristic fields associated to $\lambda_{1,8}$, $\lambda_{3,6}$, $\lambda_{2,7}$ and $\lambda_{4,5}$ are called, respectively, the fast, slow, Alfven and entropy waves. The spectral structure of system (27) is further analyzed in [4, 34].

6.1. One-dimensional tests

The one-dimensional MHD system (27) can be written in the form (1) with

$$w = \begin{pmatrix} \rho \\ \rho v_x \\ \rho v_y \\ \rho v_z \\ B_x \\ B_y \\ B_z \\ E \end{pmatrix}, \qquad F(w) = \begin{pmatrix} \rho v_x \\ \rho v_x^2 + P^* - B_x^2 \\ \rho v_x v_y - B_x B_y \\ \rho v_x v_z - B_x B_z \\ 0 \\ v_x B_y - v_y B_x \\ v_x B_z - v_z B_x \\ v_x(E + P^*) - B_x(v_x B_x + v_y B_y + v_z B_z) \end{pmatrix}. \tag{29}$$

In this case, the divergence-free condition (28) reduces to $B_x \equiv$ constant. On the other hand, the Euler equations are simply obtained by putting $B_x = B_y = B_z = 0$ in (29).

In this section we will compare the results obtained with the following schemes:

- The Roe scheme based on the Roe matrices for ideal MHD introduced in [8].
- The Osher-Solomon scheme (9) proposed by Dumbser and Toro in [19], in which the eigendecomposition is computed numerically.
- The polynomial aproximate Osher-Solomon scheme (11), using Cheyshev polynomials of order $2p = 4$.

- The rational aproximate Osher-Solomon scheme (15) based on the Newman function $R_4(x)$.
- The rational aproximate Osher-Solomon schemes (15) based on the Halley functions $H_r(x)$, for $r = 1, 2, 3$.

The above schemes will be denoted as OS, OS-Cheb-4, OS-Newman-4, and OS-Halley-r, respectively.

With respect to the high-order schemes, the third-order PHM ([28]) method has been considered, combined with a TVD Runge-Kutta method of the same order for time stepping. It is worth noticing that, in the experiments performed, PHM produces less oscillations near discontinuities than third-order WENO schemes, probably due to the local character of hyperbolic reconstructions.

6.1.1. Stationary contact discontinuity

The purpose of this test, first proposed in [21], is to study the effect of the numerical diffusion in the approximation of a stationary contact discontinuity. This effect, known as *numerical heat conduction*, may cause incorrect heating across the discontinuity; see [18] for a discussion on this topic.

The initial conditions for the Euler equations are given by

$$(\rho, v_x, P) = \begin{cases} (1, 0, 1) & \text{for } x \leq 0.5, \\ (2, 0, 1) & \text{for } x > 0.5, \end{cases}$$

with $\gamma = 1.4$. The solution consists in a stationary contact wave located at $x = 0.5$. The problem has been solved in the domain $[0, 1]$ with 200 cells and CFL=0.5 until a final time $t = 4$.

Figure 1 shows the approximations to the density component. Notice that, by design, both Roe and Osher-Solomon methods compute the solution exactly in this case. For the sake of comparison, the results obtained with the HLL solver has also been included. Regarding the first order schemes, OS-Newman-4 gives the best approximation to the solution, followed by OS-Halley-2, OS-Cheb-4 and OS-Halley-1; HLL provides a worse resolution of the discontinuity, as it is much more diffusive than any of the other schemes. This situation is mantained when third-order versions of the schemes are considered. This is more clearly seen in Figure 2, where a zoom of the top of the discontinuity is shown.

Finally, Figure 3 shows the efficiency curves for both the first and third order solvers. These curves show, in logarithmic scale, the CPU time versus the L^1 error with respect to the exact solution for four meshes with

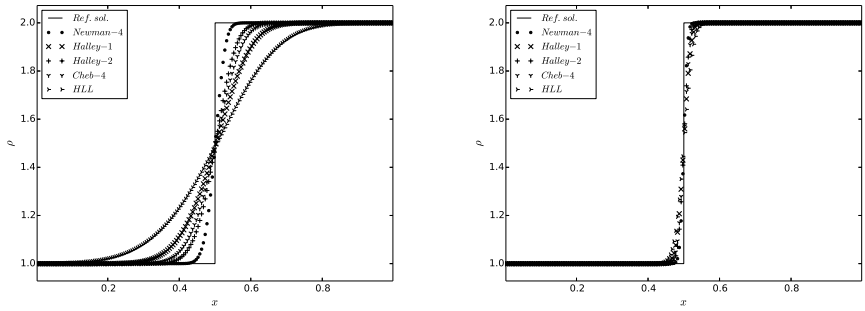

Figure 1: Test 6.1.1: Stationary contact discontinuity. Left: first order. Right: third order.

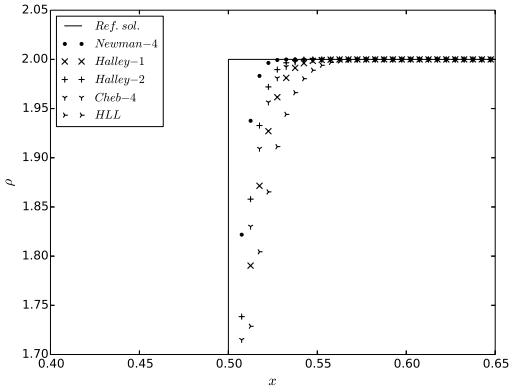

Figure 2: Test 6.1.1: Stationary contact discontinuity. Zoom of the third-order solution.

increasing number of cells (100, 200, 400, and 800). For the first order solvers, OS-Newman-4 is by far the most efficient for this problem, followed by OS-Cheb-4, OS-Halley-2, OS-Halley-1 and HLL. The situation is a little bit different when going to third order: OS-Newman-4 is again the most efficient solver, followed by OS-Cheb-4, HLL, OS-Halley-2 and OS-Halley-1. In particular, this test shows that the choice of an appropriate first-order solver is important even when it is going to be used as a building block for higher-order schemes.

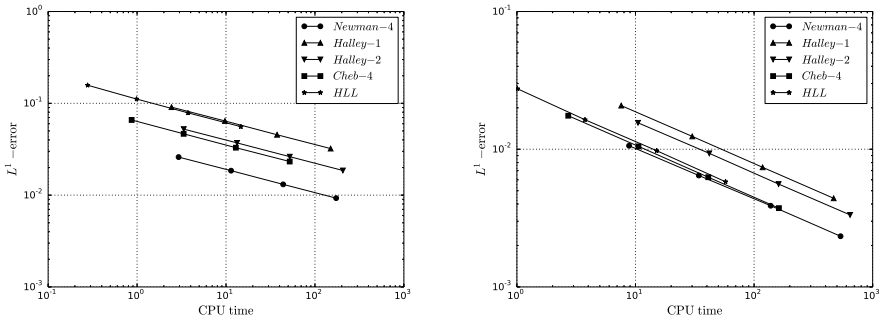

Figure 3: Test 6.1.1: Efficiency curves CPU vs. L^1-error. Left: first order. Right: third order.

6.1.2. Overheating error

The following initial conditions for the Euler equations are considered:

$$(\rho, v_x, P) = \begin{cases} (1, 1, 10^{-3}) & \text{for } x \leq 0.5, \\ (1, -1, 10^{-3}) & \text{for } x > 0.5, \end{cases}$$

with $\gamma = 5/3$. This test was proposed in [21]; see also [18]. The solution consists in two shock waves generated by the initial jump in velocity. These waves travel in opposite directions from the center of the domain, while the gas remains at rest between them. It is known that most standard schemes present a numerical pathology known as *overheating*, in which the density error around the shock point induces an excessive increase of the internal energy. The overheating error is $\mathcal{O}(1)$ independently of the discretization.

The solutions have been computed until time $t = 0.4$ in the interval $[0, 1]$ using 200 cells and $\Delta t/\Delta x = 0.1$. Figure 4 shows a zoom of the collision zone. In the first order case, Roe and OS give the best approximations, followed by OS-Newman-4 (however, although it is not shown in the picture, it is interesting to remark that OS-Newman-8 provides as good results as Roe's method), OS-Halley-3 and OS-Cheb-4. Any of these schemes provide a much better resolution of the shocks than HLL, which is very diffusive.

With respect to the third-order schemes, some expected oscillations are observed near the shocks. However, the Roe and Osher-Solomon schemes produce additional overshoots at the shocks, which are not present in the other schemes.

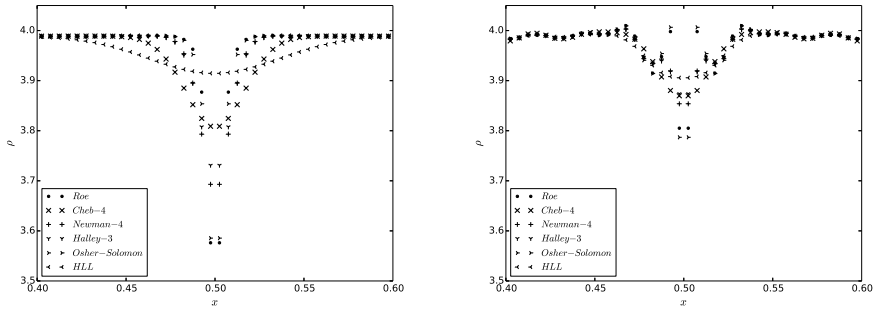

Figure 4: Test 6.1.2: Zoom of the collision of two equal strength shocks. Left: first order. Right: third order.

6.1.3. Brio-Wu shock tube problem

The following test was proposed in [4] to show the formation of a compound wave consisting of a shock followed by a rarefaction wave. The solution of the problem is composed by five constant states separated by a left-moving fast rarefaction wave, a slow compound wave, a contact discontinuity, a right-moving slow shock and a right-moving fast rarefaction wave. The initial conditions for the MHD system are the following:

$$(\rho, v_x, v_y, v_z, B_x, B_y, B_z, P) = \begin{cases} (1, 0, 0, 0, 0.75, 1, 0, 1) & \text{for } x \leq 0, \\ (0.125, 0, 0, 0, 0.75, -1, 0, 0.1) & \text{for } x > 0, \end{cases}$$

with $\gamma = 2$. The problem has been solved until time $t = 0.2$ in the interval $[-1, 1]$ with a 1000 cell spatial discretization and CFL=0.8. As it can be seen in Figure 5, in this case there are no appreciable differences between the solutions computed with Roe, OS-Newman-4, OS-Halley-2, OS-Cheb-4 and OS, both in first and third orders: all the schemes perform equally well. On the other hand, the first order HLL method provides a worse resolution of the compound wave, which is however improved in third order. Finally, Table 1 shows the relative CPU times with respect to the first-order OS scheme.

6.2. Two-dimensional tests

Consider the two-dimensional MHD system (27), that can be written in the form

$$\partial_t w + \partial_x F(w) + \partial_y G(w) = 0, \tag{30}$$

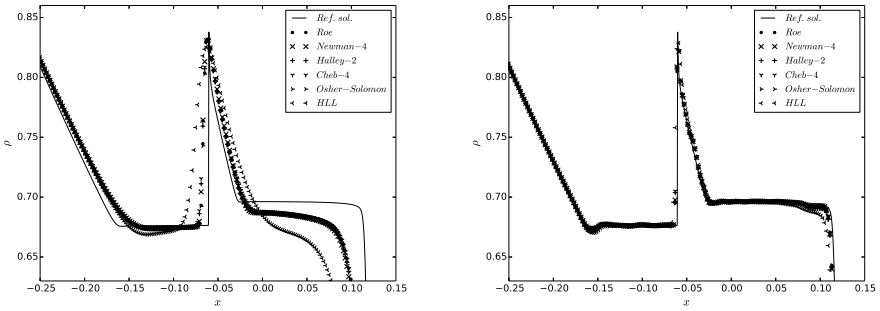

Figure 5: Test 6.1.3: Zoom of the density compound wave. Left: first order. Right: third order.

Table 1: Test 6.1.3: Relative CPU times with respect to the first-order OS solver.

Method	CPU (first order)	CPU (third order)
OS	1.00	3.11
OS-Cheb-4	0.08	0.26
OS-Newman-4	0.28	0.88
OS-Halley-1	0.24	0.73
OS-Halley-2	0.32	1.00
Roe	0.38	1.12
HLL	0.02	0.09

where the state w and the x-flux $F(w)$ are given by (29), and the y-flux $G(w)$ is defined as

$$G(w) = \begin{pmatrix} \rho v_y \\ \rho v_x v_y - B_x B_y \\ \rho v_y^2 + P^* - B_y^2 \\ \rho v_y v_z - B_y B_z \\ v_y B_x - v_x B_y \\ 0 \\ v_y B_z - v_z B_y \\ v_y(E + P^*) - B_y(v_x B_x + v_y B_y + v_z B_z) \end{pmatrix}.$$

The detailed spectral decomposition of the system can be found in [34]. To ensure the stability and accuracy of the numerical schemes, it is essential

to enforce the divergence-free constraint (28) on the magnetic field. This is done here using the technique proposed in [3], where a correction is applied at the end of every time step. Specifically, the magnetic field $\mathbf{B}$ is modified as $\mathbf{B}^c = \mathbf{B} + \nabla\phi$, where ϕ is a solution of the Poisson problem $\Delta\phi + \nabla\cdot\mathbf{B} = 0$, which is computed here with a finite difference method. For high-order schemes, the correction is performed at the end of each stage of the Runge-Kutta method used for time stepping.

For high-order schemes, the third-order polynomial reconstruction introduced in [22] has been considered. This is a WENO-type fully two-dimensional reconstruction operator having a compact stencil, which results in highly stable numerical schemes. The numerical experiments have been performed using structured meshes, although they can be designed on general nonuniform quadrilateral meshes following the guidelines in [10] and [22].

6.2.1. Smooth isentropic vortex

The purpose of this test is to analyze the convergence and stability of the proposed numerical schemes. Specifically, the smooth two-dimensional convected isentropic vortex for the Euler equations proposed in [24] is considered. Specifically, the initial condition consists in a linear perturbation of an homogeneous state, of the form

$$(\rho, v_x, v_y, P) = (1+\delta\rho, 1+\delta v_x, 1+\delta v_y, 1+\delta P).$$

Denoting $r^2 = (x-5)^2 + (y-5)^2$, the perturbations of velocity, density and pressure are given by

$$\begin{pmatrix}\delta v_x \\ \delta v_y\end{pmatrix} = \frac{\varepsilon}{2\pi} e^{\frac{1-r^2}{2}} \begin{pmatrix}5-y \\ x-5\end{pmatrix}, \quad \delta\rho = (1+\delta T)^{\frac{1}{\gamma-1}} - 1, \quad \delta P = (1+\delta T)^{\frac{\gamma}{\gamma-1}} - 1,$$

being

$$\delta T = -\frac{(\gamma-1)\varepsilon^2}{8\gamma\pi^2} e^{1-r^2}$$

the temperature perturbation. The values $\varepsilon = 5$ and $\gamma = 1.4$ have been used.

The problem has been solved in the computational domain $\mathcal{O} = [0,10] \times [0,10]$ with periodic boundary conditions and CFL=0.8. It is clear that the exact solution of the problem is simply the initial condition convected with the mean velocity. In Table 2 are shown the L^1 errors and orders obtained after one time period at $t = 10$ with the third-order OS-Cheb-4,

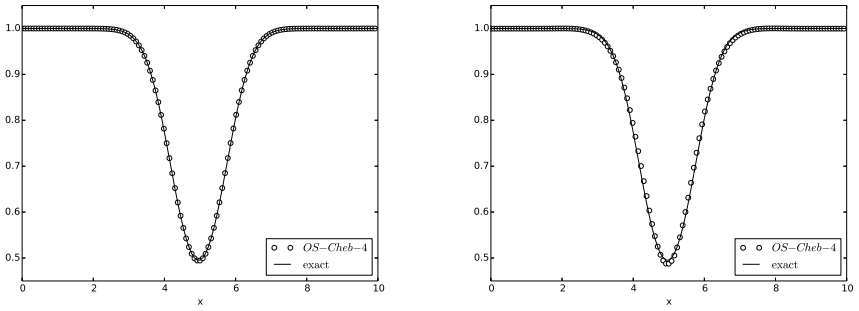

Figure 6: Test 6.2.1: Density cut in the x-direction, computed with the third-order OS-Cheb-4 scheme. Left: time $t = 10$. Right: time $t = 100$.

OS-Newman-4, OS-Halley-2 and OS schemes, relative to the density component. As it can be seen, all the proposed schemes give similar results as the Osher-Solomon method. We remark again that the advantage of our schemes is that the eigenstructure of the system need not to be known.

On the other hand, the solution has been calculated at time $t = 100$, after ten time periods. Figure 6 shows a cut through the center of the vortex in the x-direction for the density variable. The solution has been computed with the third-order OS-Cheb-4 method using 128 cells, although any of the other schemes gives a similar result. As it can be observed, the dissipation is very small in this case.

6.2.2. Orszag-Tang vortex

The Orszag-Tang vortex system ([30]) has been widely analyzed in the literature, as it provides a model of complex flow containing many significant features of MHD turbulence. Starting from a smooth state, the system develops complex interactions between different shock waves generated as the system evolves in the transition to turbulence.

The initial data proposed in [40] has been considered: for $(x, y) \in [0, 2\pi] \times [0, 2\pi]$, we take

$$\rho(x, y, 0) = \gamma^2, \quad v_x(x, y, 0) = -\sin(y), \quad v_y(x, y, 0) = \sin(x),$$
$$B_x(x, y, 0) = -\sin(y), \quad B_y(x, y, 0) = \sin(2x), \quad P(x, y, 0) = \gamma,$$

with $\gamma = 5/3$. Periodic boundary conditions are imposed in the x- and y-directions. The computations have been done using a 192×192 uniform mesh and CFL=0.8.

Table 2: Test 6.2.1: Third order results for the density component ρ at time $t = 10$.

	OS-Cheb-4		OS-Newman-4	
N	L^1 error	L^1 order	L^1 error	L^1 order
16	1.47E+00	–	1.47E+00	–
32	7.77E–01	0.92	7.95E–01	0.89
64	1.98E–01	1.97	2.03E–01	1.97
128	1.37E–02	3.85	1.39E–02	3.87
	OS-Halley-2		Osher-Solomon	
N	L^1 error	L^1 order	L^1 error	L^1 order
16	1.46E+00	–	1.45E+00	–
32	7.81E–01	0.90	7.95E–01	0.87
64	1.95E–01	2.00	1.96E–01	2.02
128	1.33E–02	3.87	1.33E–02	3.88

Figure 7 shows the results obtained with the third-order OS-Cheb-4 scheme at times $t = 0.5$, $t = 2$ and $t = 3$, for the density and pressure components (analogous solutions are obtained with the third-order OS-Newman-4, OS-Halley-2, and OS schemes). The results are in very good agreement with those presented in [25, 26], which shows that our schemes are robust and accurate enough to resolve the complicated structure of this vortex system. Finally, Table 3 shows the relative CPU times with respect to the first-order OS scheme.

Table 3: Test 6.2.2: Relative CPU times with respect to the first-order OS solver. Final time: $t = 0.2$.

Method	CPU (first order)	CPU (third order)
OS	1.00	5.82
OS-Cheb-4	0.16	1.04
OS-Newman-4	0.38	2.32
OS-Halley-2	0.50	2.79

6.2.3. The rotor problem

In this section we consider the rotor problem proposed in [1]; see also [38]. Initially, there is a dense rotating disk at the center of the domain,

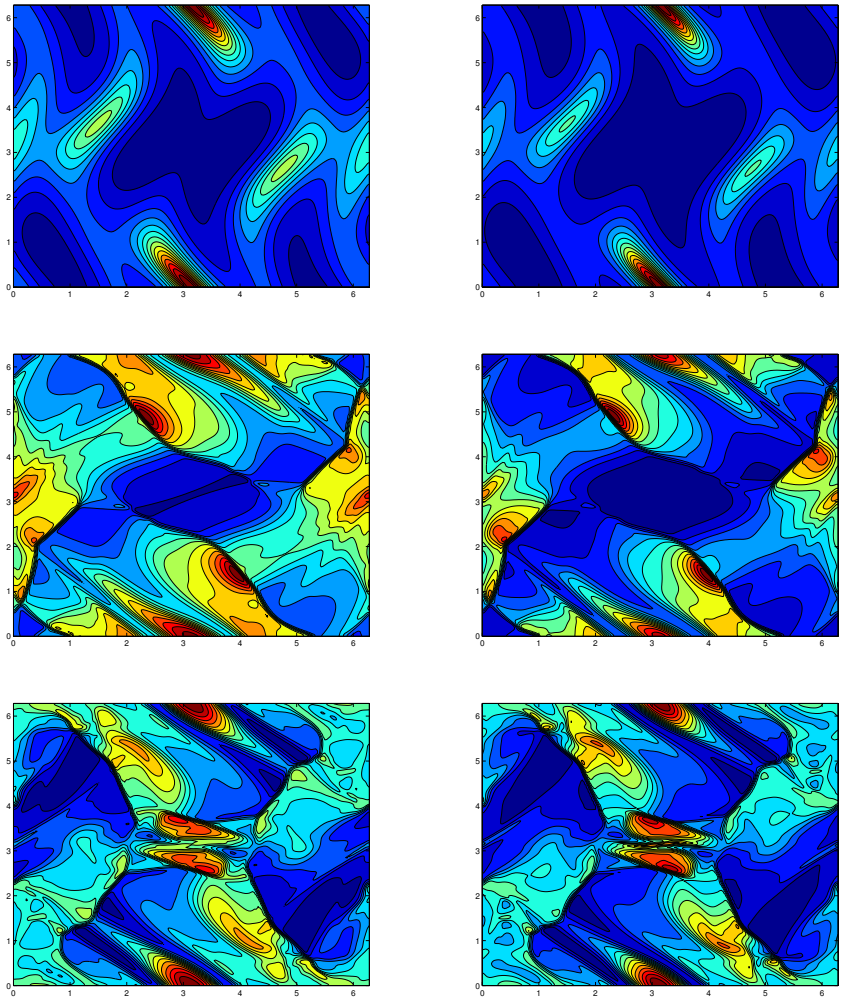

Figure 7: Test 6.2.2: Evolution of the Orszag-Tang vortex. Density (left) and pressure (right) computed at times (from top to bottom) $t = 0.5$, $t = 2$ and $t = 3$. Results obtained with the third-order OS-Cheb-4 scheme with 192×192 cells.

while the ambient fluid remains at rest. These two areas are connected by means of a taper function, which helps to reduce the initial transient. Since the centrifugal forces are not balanced, the rotor is not in equilibrium. The rotating dense fluid will be confined into an oblate shape, due to the action of the magnetic field.

The computational domain is $[0,1]\times[0,1]$ with periodic boundary conditions. Define $r_0 = 0.1$, $r_1 = 0.115$, $f = (r_1 - r)/(r_1 - r_0)$ and $r = [(x-0.5)^2 + (y-0.5)^2]^{1/2}$; then, the initial conditions are given by

$$(\rho(x,y), v_x(x,y), v_y(x,y)) = \begin{cases} (10, -(y-0.5)/r_0, (x-0.5)/r_0) & \text{if } r < r_0, \\ (1+9f, -(y-0.5)f/r, (x-0.5)f/r) & \text{if } r_0 < r < r_1, \\ (1,0,0) & \text{if } r > r_1, \end{cases}$$

with $B_x = 2.5/\sqrt{4\pi}$, $B_y = 0$ and $P = 0.5$. We take $\gamma = 5/3$.

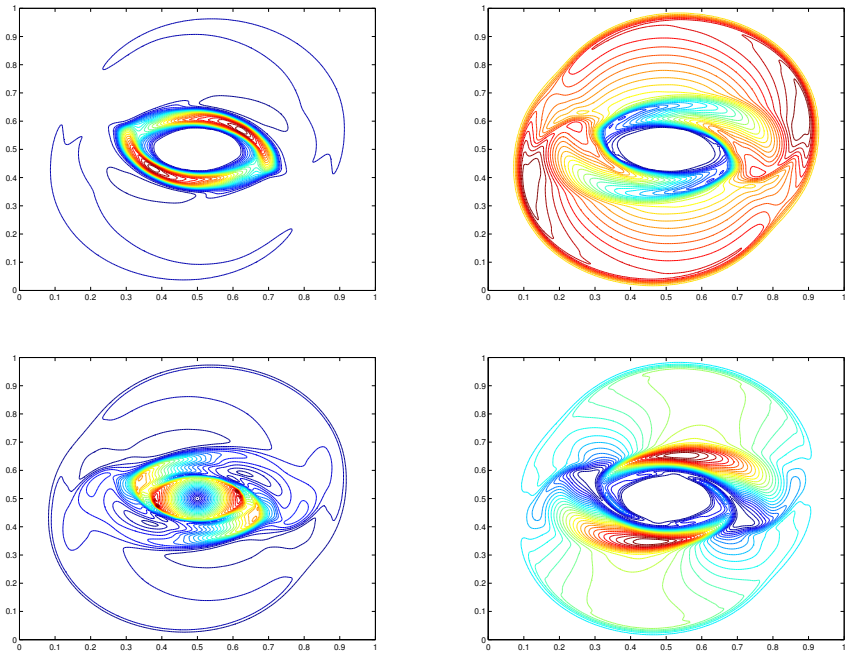

Figure 8: Test 6.2.3: Density ρ (top left), pressure P (top right), Mach number $|\mathbf{v}|/a$ (bottom left) and magnetic pressure $|\mathbf{B}|^2/2$ (bottom right) computed at time $t = 0.295$. Results obtained with the third-order OS-Cheb-4 scheme with 200×200 cells.

Figure 8 shows the solutions obtained with the third order OS-Cheb-4 scheme at time $t = 0.295$ on a 200×200 mesh with CFL$= 0.8$. The results are in good agreement with those in [1, 26, 38]. As in the previous tests, OS-Newman-4 and OS-Halley-2 give similar results as OS-Cheb-4. On the contrary, the OS scheme fails for this problem around time $t \approx 0.187$.

Finally, Figure 9 shows a comparison between the third-order OS-Cheb-4 and HLL methods. As it can be seen, HLL produces less precise results than OS-Cheb-4, which shows that the choice of the first order solver is important even when using high-order schemes.

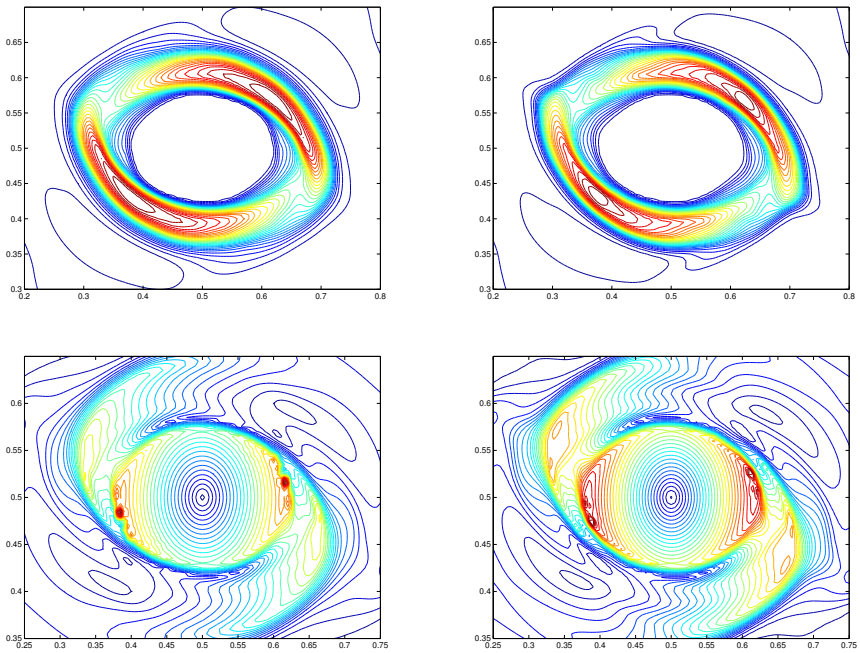

Figure 9: Test 6.2.3: Comparison between the solutions obtained with the third-order HLL (left) and OS-Cheb-4 (right) schemes. Top: density. Bottom: Mach number.

6.2.4. 2d Riemann problem

We consider the two-dimensional Riemann problem proposed in [16], whose initial data is given in Table 4. The initial condition is chosen so that the magnetic field is divergence free and the solutions of three of the four one-dimensional Riemann problems are simple waves. In particular, denoting the quadrants by Roman numbers as in Table 4, there is a rarefaction wave for the problem I↔II and shocks for II↔III and III↔IV.

The problem has been solved in the computational domain $[-1,1] \times [-1,1]$ until a final time $t = 0.2$, using a 200×200 cartesian mesh, $\gamma = 5/3$ and CFL=0.8. As in [26], Neumann boundary conditions have been

Table 4: Test 6.2.4: Initial data for the 2d Riemann problem.

Quadrant	ρ	ρv_x	ρv_y	ρv_z	B_x	B_y	B_z	E
I: $x > 0$, $y > 0$	0.9308	1.4557	-0.4633	0.0575	0.3501	0.9830	0.3050	5.0838
II: $x < 0$, $y > 0$	1.0304	1.5774	-1.0455	-0.1016	0.3501	0.5078	0.1576	5.7813
III: $x < 0$, $y < 0$	1.0000	1.7500	-1.0000	0.0000	0.5642	0.5078	0.2539	6.0000
IV: $x > 0$, $y < 0$	1.8887	0.2334	-1.7422	0.0733	0.5642	0.9830	0.4915	12.999

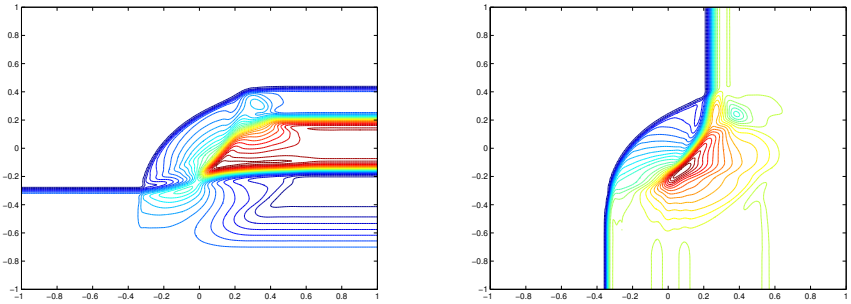

Figure 10: Test 6.2.4: Contours at time $t = 0.2$ obtained with the third-order OS-Cheb-4 scheme. Left: B_x. Right: B_y.

considered. Figure 10 shows the contours of B_x and B_y computed with the third order OS-Cheb-4 scheme. As it was reported in [16], some schemes have problems with keeping B_y constant across the shock in II↔III. Moreover, they produce strong distortions in B_x and B_y behind the rarefaction wave in I↔II. As it can be observed in Figure 10, our schemes do not suffer from any of these pathologies, and the obtained results can be directly compared with those in [16, 26]. The OS-Newman-4, OS-Halley-2 and OS schemes produce very similar results for the B_x component, but there are some differences with respect to B_y. This is shown in Figure 11: in this case the OS scheme seems to produce the less precise results.

Finally, we compare the quality of the solution of the I↔IV Riemann problem at $x = 0.93$, as it is done in [16, 26]. Figure 12 shows a comparison between the solution of the two-dimensional Riemann problem obtained with OS-Cheb-4 at $x = 0.93$ and a one-dimensional reference solution. In this

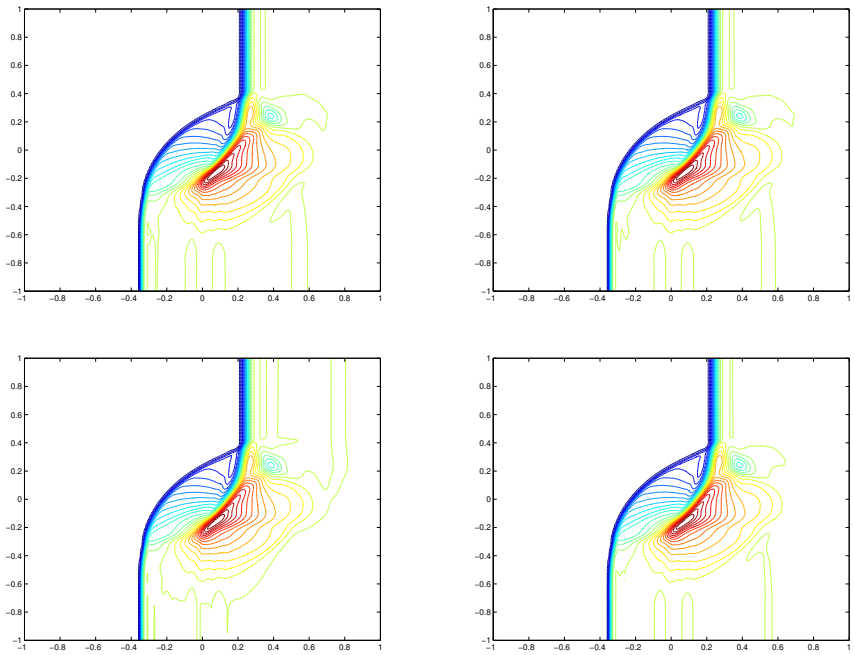

Figure 11: Test 6.2.4: Contours for B_y computed with several schemes. Top left: OS-Newman-4. Top right: OS-Halley-2. Bottom left: OS. Bottom right: OS-Cheb-4.

case, OS-Newman-4, OS-Halley-2 and OS give similar results.

7. Applications to the two-layer shallow water system

The equations of a two-layer shallow flow are considered in this section to test the behavior of the approximate Osher-Solomon schemes in the non-conservative case, as they constitute a representative model including both source and nonconservative coupling terms.

The equations governing the one-dimensional flow of two superposed

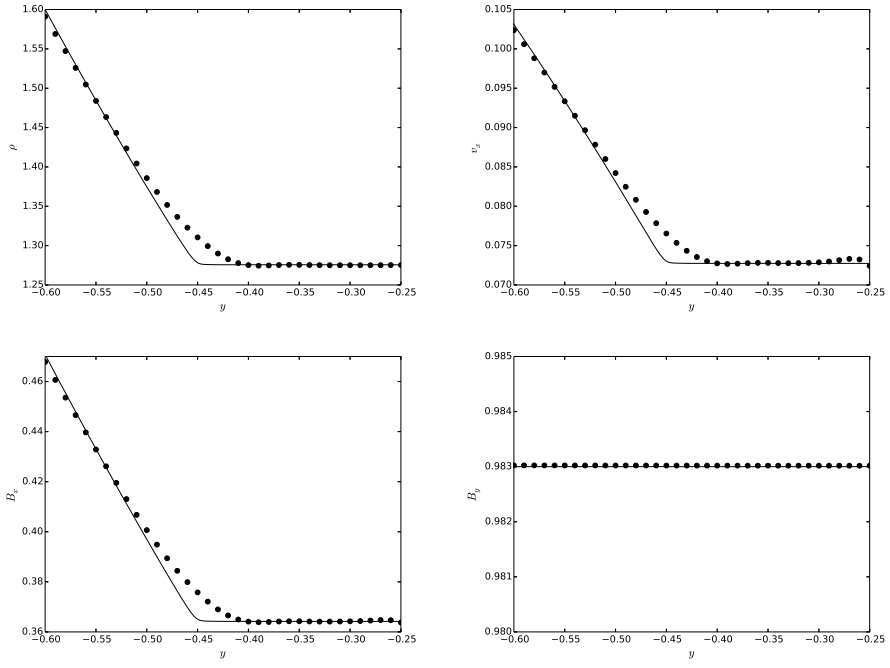

Figure 12: Test 6.2.4: Cuts at $x = 0.93$ and $t = 0.2$, with $y \in [-0.6, -0.2]$. Solid line: reference solution. Dots: OS-Cheb-4. Top left: ρ. Top right: v_x. Bottom left: B_x. Bottom right: B_y.

inmiscible layers of shallow water fluids are given by ([14])

$$\begin{cases} \partial_t h_1 + \partial_x q_1 = 0, \\ \partial_t q_1 + \partial_x \left(\dfrac{q_1^2}{h_1} + \dfrac{g}{2} h_1^2 \right) + g h_1 \partial_x \big(h_2 - H \big) = 0, \\ \partial_t h_2 + \partial_x q_2 = 0, \\ \partial_t q_2 + \partial_x \left(\dfrac{q_2^2}{h_2} + \dfrac{g}{2} h_2^2 \right) + g h_2 \partial_x \big(r h_1 - H \big) = 0, \end{cases} \tag{31}$$

where h_j are the fluid depths, $q_j = h_j u_j$ are the discharges (u_j being the velocities), and $H(x)$ represents the depth function measured from a fixed level of reference; g is the gravity constant and $r = \rho_1/\rho_2$ is the ratio of densities (it is assumed that each layer have a constant density ρ_j). Notice that index $j = 1$ corresponds to the upper layer and $j = 2$ to the lower one.

System (31) can be written in the nonconservative form (23) by taking

$$w = \begin{pmatrix} h_1 \\ q_1 \\ h_2 \\ q_2 \end{pmatrix}, \quad F(w) = \begin{pmatrix} q_1 \\ \frac{q_1^2}{h_1} + \frac{g}{2}h_1^2 \\ q_2 \\ \frac{q_2^2}{h_2} + \frac{g}{2}h_2^2 \end{pmatrix}, \quad G(w) = \begin{pmatrix} 0 \\ gh_1 \\ 0 \\ gh_2 \end{pmatrix},$$

and

$$B(w) = \begin{pmatrix} 0 & 0 & 0 & 0 \\ 0 & 0 & gh_1 & 0 \\ 0 & 0 & 0 & 0 \\ rgh_2 & 0 & 0 & 0 \end{pmatrix}.$$

Remark 5. It is possible to build a Roe matrix for system (31), although its eigenstructure is not explicitely known ([33]). Therefore, the implementation of Roe's method requires the numerical approximation of eigenvalues and eigenvectors, which in practice is done using some standard numerical library. □

To build the approximate Osher-Solomon fluxes (26), it is necessary to define the elements $B_{i+1/2}$ and $G_{i+1/2}$. The matrix $B_{i+1/2}$ is given by ([14])

$$B_{i+1/2} = \begin{pmatrix} 0 & 0 & 0 & 0 \\ 0 & 0 & gh_{1,i+1/2} & 0 \\ 0 & 0 & 0 & 0 \\ rgh_{2,i+1/2} & 0 & 0 & 0 \end{pmatrix},$$

where

$$h_{k,i+1/2} = \frac{h_{k,i} + h_{k,i+1}}{2}, \quad k = 1, 2.$$

The vector $G_{i+1/2}$ can be taken as

$$G_{i+1/2} = \begin{pmatrix} 0 \\ gh_{1,i+1/2} \\ 0 \\ gh_{2,i+1/2} \end{pmatrix}.$$

Finally, a first order approximation of the maximum wave speed is given by ([14])

$$|\lambda_{i+1/2,\max}| \approx |\bar{u}_{i+1/2}| + c_{i+1/2},$$

where

$$\bar{u}_{i+1/2} = \frac{q_{1,i+1/2} + q_{2,i+1/2}}{h_{1,i+1/2} + h_{2,i+1/2}}, \quad c_{i+1/2} = \sqrt{g(h_{1,i+1/2} + h_{2,i+1/2})}.$$

With respect to the numerical methods, OS-Cheb-4, OS-Newman-4, OS-Halley-2, OS, and the standard HLL scheme will be compared in this section. As in Section 6, PHM spatial reconstructions and third-order TVD Runge-Kutta time stepping will be used for high-order schemes.

7.1. Internal dam break

This test, which have been taken from [11], simulates a dam break in a two-layer system. The initial conditions are given by

$$h_1(x,0) = \begin{cases} 0.9 & \text{if } x < 5, \\ 0.1 & \text{if } x \geq 5, \end{cases} \qquad h_2(x,0) = 1 - h_1(x,0),$$

and $q_1(x,0) = q_2(x,0) = 0$, for $x \in [0,10]$. The ratio of densities has been taken as $r = 0.99$. The problem has been solved using a mesh with 200 grid points until time $t = 20$, with CFL number 0.9. Open boundary conditions have been imposed.

Figure 13 compares the results obtained. As it can be seen, in first order the best results are obtained with the OS-Newman-4 and OS schemes, followed by OS-Halley-2 and OS-Cheb-4, while HLL is not able to capture the structure of the interface. On the other hand, in third order all the schemes perform equally well, being HLL the one that gives the less precise results.

7.2. Transcritical flux with shock

The initial condition for this test, previously considered in [12], consists in an internal dam break over a non-flat bottom, that eventually produces a stationary transcritical solution with a shock. Specifically, the initial conditions are given by $q_1(x,0) = q_2(x,0) = 0$,

$$h_1(x,0) = \begin{cases} 0.48 & \text{for } x < 0, \\ 0.02 & \text{for } x \geq 0, \end{cases} \qquad h_2(x,0) = H(x) - h_1(x,0),$$

and the bottom topography is defined by

$$H(x) = 1 - \frac{1}{2}e^{-x^2}, \quad x \in [-5,5].$$

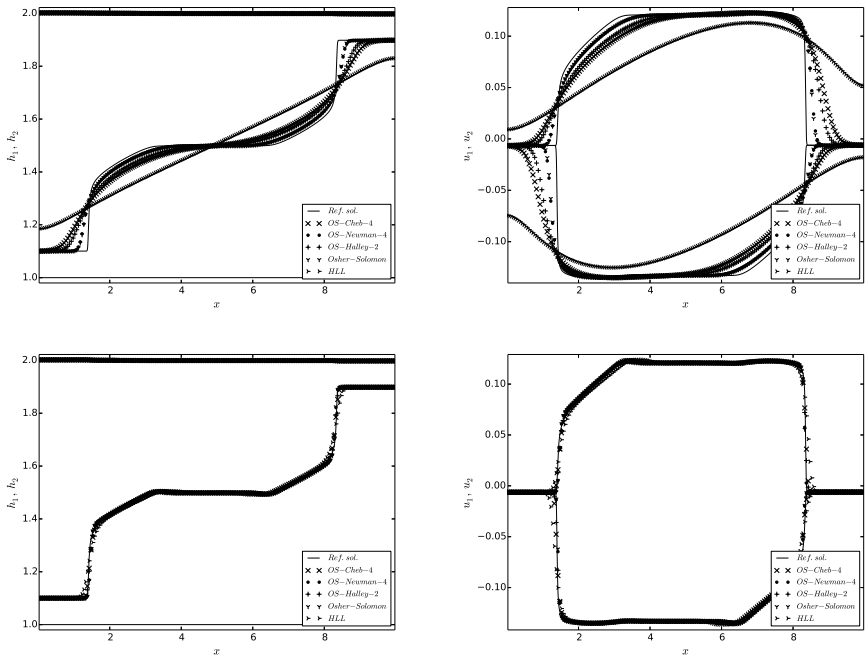

Figure 13: Test 7.1. Left: heights. Right: velocities. Top: first order . Bottom: third order.

Open wall boundary conditions have been imposed, and the ratio of densities has been chosen as $r = 0.998$.

The numerical solutions have been computed on a mesh with 200 grid points until time $t = 100$, with CFL number 0.9. Figure 14 shows the results obtained, where the reference solution has been calculated using Roe's method with 12800 points. As it can be observed, in first order the OS-Newman-4 and OS schemes provide the best resolution of the interface, followed by OS-Halley-2 and OS-Cheb-4; on the other hand, HLL is unable to resolve the complex structure of the interface. Of course, the situation improves when the third-order versions of the schemes are used. However, it should be noted that HLL presents a worse resolution near discontinuities than any of the other schemes considered. This is better seen in Figure 15, where a closer view of the shock has been plotted. This fact indicates that the choice of the first order solver to be used as building block in high-order schemes is important, specially when the solution presents complex features. Also in Figure 15 it is seen that although the third-order OS-Newman-4 and

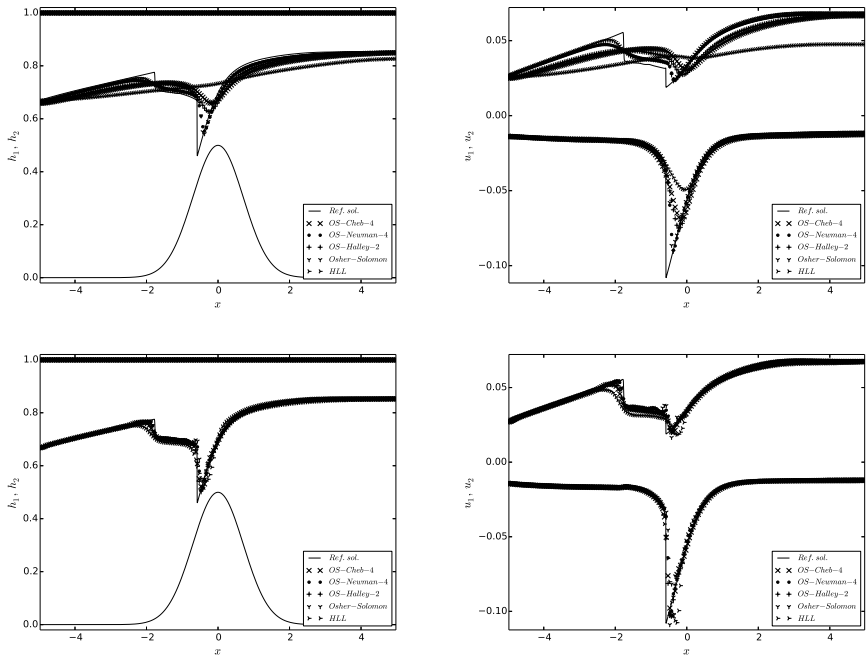

Figure 14: Results for test 7.2. Left: free surface, interface and bottom. Right: velocities. Top: first order. Bottom: third order

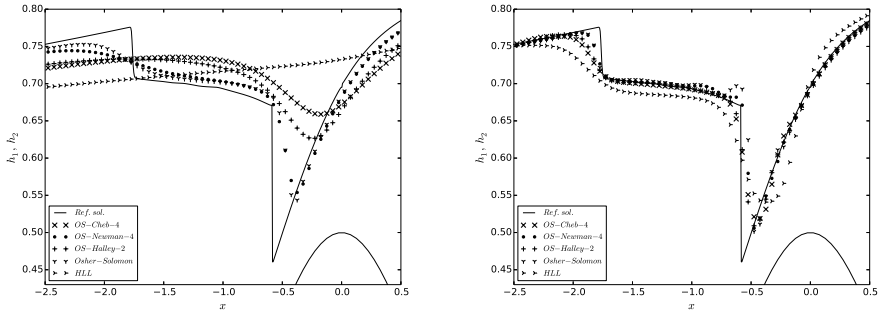

Figure 15: Closer view of the shock at the interface in test 7.2. Left: first order. Right: third order.

OS schemes perform similarly, OS presents more pronounced oscillations near the shock. Finally, the relative CPU times with respect to the first-

order OS scheme are shown in Table 5.

Table 5: Test 7.2: Relative CPU times with respect to the first-order OS solver.

Method	CPU (first order)	CPU (third order)
OS	1.00	2.98
OS-Cheb-4	0.15	0.51
OS-Newman-4	0.37	1.17
OS-Halley-2	0.44	1.39
HLL	0.06	0.24

8. Conclusions

We have proposed a new kind of Riemann solvers for conservative and nonconservative hyperbolic systems, which are based on a simplified version of the classical Osher-Solomon scheme. The Osher-Solomon solver relies on the evaluation of the integral of the absolute value matrix of the flux Jacobian through a path linking states in phase space. This integral can be approximated by an appropriate quadrature formula, as it was also done in [19, 20]. To avoid the evaluation of the absolute value matrices at the quadrature points, which would require the computation of the eigenstructure of the system, we have proposed several ways to approximate them accurately and efficiently. In particular, Chebyshev polynomial approximations and two kinds of rational approximations (based on Newman and Halley functions) have been considered. To construct the associated approximate Osher-Solomon schemes, only a bound on the spectral radius of the Jacobian is needed. The proposed schemes have been compared with the Osher-Solomon scheme proposed in [19, 20], Roe and HLL. An additional feature of our schemes is that no entropy-fix is needed.

Different initial value Riemann problems for ideal gas dynamics, magnetohydrodynamics and multilayer shallow water equations have been considered to test the performances of the approximate Osher-Solomon schemes. The numerical tests indicate that the proposed schemes are robust, stable and accurate with a satisfactory time step restriction. In particular, rational-based methods are found to be superior for problems with a complex internal wave pattern. Approximate Osher-Solomon schemes thus provide an efficient alternative when approximating time-dependent solutions in which the spectral decomposition is complex or computationally expensive.

Appendix A. Implementation of the OS-Chebyshev scheme

Consider the numerical flux (11) written as

$$F_{i+1/2} = \frac{F(w_i) + F(w_{i+1})}{2} - \frac{1}{2}\sum_{k=1}^{q} \omega_k \big(\widetilde{P}^{(k)}_{i+1/2}(w_{i+1} - w_i)\big). \qquad \text{(A-1)}$$

It is clear that the matrices $\widetilde{P}^{(k)}_{i+1/2}$ need not to be computed explicitely, as only the vectors $\widetilde{P}^{(k)}_{i+1/2}(w_{i+1} - w_i)$ are involved in the flux formula. For the sake of clarity, the index i will be dropped in what follows, unless necessary. Then, we focus on the computation of

$$\widetilde{P}^{(k)}\Delta w = |\lambda^{(k)}_{\max}| P\big(|\lambda^{(k)}_{\max}|^{-1} A^{(k)}\big)\Delta w, \quad k = 1, \ldots, q,$$

where $\Delta w = w_{i+1} - w_i$ and $\lambda^{(k)}_{\max}$ is the eigenvalue of $A^{(k)} = A(w_i + s_k(w_{i+1} - w_i))$ with the largest absolute value (see Section 4).

The Chebyshev polynomial $P(x) = \tau_{2p}(x)$ is given by (13), so we can write

$$\widetilde{P}^{(k)}\Delta w = |\lambda^{(k)}_{\max}| \left(\alpha_0 \Delta w + \sum_{j=1}^{p} \alpha_j W^{[2j]}\right), \qquad \text{(A-2)}$$

where

$$\alpha_0 = \frac{2}{\pi}, \qquad \alpha_j = \frac{4}{\pi}\frac{(-1)^{j+1}}{(2j-1)(2j+1)}, \quad j = 1, \ldots, p,$$

and the vectors $W^{[2j]}$ are given by

$$W^{[2j]} = T_{2j}\big(|\lambda^{(k)}_{\max}|^{-1} A^{(k)}\big)\Delta w.$$

From (14), $W^{[2j]}$ can be recursively defined as follows:

- $W^{[0]} = \Delta w$.
- $W^{[2]} = 2|\lambda^{(k)}_{\max}|^{-2}\big(A^{(k)}\big)^2 \Delta w - \Delta w$.
- $W^{[2j]} = 4|\lambda^{(k)}_{\max}|^{-2}\big(A^{(k)}\big)^2 W^{[2j-2]} - 2W^{[2j-2]} - W^{[2j-4]}$, for $j \geq 2$.

The above expressions allow an efficient implementation of the OS-Chebyshev method. This is the form in which the numerical experiments in Sections 6 and 7 have been performed.

In many cases, the Jacobian matrix $A(w)$ may be difficult or expensive to compute, so from a practical point of view it is interesting to implement

the scheme without explicitely calculating the Jacobian. Following [37], the product of the Jacobian $A(w)$ by a given vector v can be expressed using the finite difference formulation

$$A(w)v = \frac{\partial F}{\partial w}(w)v = \lim_{\varepsilon \to 0} \frac{F(w+\varepsilon v) - F(w)}{\varepsilon},$$

which leads to the following approximation:

$$A(w)^2 v \approx \frac{F\big(w + F(w+\varepsilon v) - F(w)\big) - F(w)}{\varepsilon},$$

where ε has to be chosen small relative to the norm of w. Then, the vector $W^{[2j]}$ is now given by

$$\begin{aligned} W^{[2j]} =& \frac{4}{\varepsilon |\lambda_{\max}^{(k)}|^2} \Big(F\big(w^{(k)} + F(w^{(k)} + \varepsilon W^{[2j-2]}) - F(w^{(k)})\big) - F(w^{(k)}) \Big) \\ & - 2W^{[2j-2]} - W^{[2j-4]}, \end{aligned} \tag{A-3}$$

where $w^{(k)} = w_i + s_k(w_{i+1} - w_i)$; $W^{[2]}$ is redefined in a similar way. Thus, expressions (A-1), (A-2) and (A-3) provide a free-Jacobian implementation of the OS-Chebyshev scheme, in which only evaluations of the flux function $F(w)$ are involved.

References

[1] D.S. Balsara, D.S. Spicer, A staggered mesh algorithm using high order Godunov fluxes to ensure solenoidal magnetic fields in magnetohydrodynamic simulations, J. Comput. Phys. 149 (1999) 270–292.

[2] S. Bernstein, Sur la meilleure approximation de $|x|$ par del polynômes de degrés donés, Acta Math. 37 (1913) 1–57.

[3] J.U. Brackbill, J.C. Barnes, The effect of nonzero $\nabla \cdot B$ on the numerical solution of the magnetohydrodynamic equations, J. Comput. Phys. 35 (1980) 426–430.

[4] M. Brio, C.C. Wu, An upwind differencing scheme for the equations of ideal magnetohydrodynamics, J. Comput. Phys. 75 (1988) 400–422.

[5] L. Brutman, On rational interpolation to $|x|$ at the adjusted Chebyshev nodes, J. Approx. Theory 95 (1998) 146–152.

[6] L. Brutman, E. Passow, Rational interpolation to $|x|$ at the Chebyshev nodes, Bull. Austral. Math. Soc. 56 (1997) 81–86.

[7] V. Candela, A. Marquina, Recurrence relations for rational cubic methods I: the Halley method, Computing 44 (1990) 169–184.

[8] P. Cargo, G. Gallice, Roe matrices for ideal MHD and systematic construction of Roe matrices for systems of conservation laws, J. Comput. Phys. 136 (1997) 446–466.

[9] M.J. Castro Díaz, E.D. Fernández-Nieto, A class of computationally fast first order finite volume solvers: PVM methods, SIAM J. Sci. Comput. 34 (2012) A2173–A2196.

[10] M.J. Castro Díaz, E.D. Fernández-Nieto, A.M. Ferreiro, J.A. García, C. Parés, High order extensions of Roe schemes for two dimensional nonconservative hyperbolic systems, J. Sci. Comput. 39 (2009) 67–114.

[11] M.J. Castro Díaz, E.D. Fernández-Nieto, G. Narbona-Reina, M. de la Asunción, A second order PVM flux limiter method. Application to magnetohydrodynamics and shallow stratified flows, J. Comput. Phys. 262 (2014) 172–193.

[12] M.J. Castro, J.M. Gallardo, A. Marquina, A class of incomplete Riemann solvers based on uniform rational approximations to the absolute value function, J. Sci. Comput. 60 (2014) 363–389.

[13] M.J. Castro, J.M. Gallardo, C. Parés, High order finite volume schemes based on reconstruction of states for solving hyperbolic systems with nonconservative products. Applications to shallow-water systems, Math. Comp. 75 (2006) 1103–1134.

[14] M.J. Castro, J. Macías, C. Parés, A Q-scheme for a class of systems of coupled conservation laws with source term. Application to a two-layer 1-d shallow water system. Math. Mod. Num. Anal. 35 (2001) 107–127.

[15] F. Cordier, P. Degond, A. Kumbaro, Phase appearance or disappearance in two-phase flows, J. Sci. Comput. 58 (2014) 115–148.

[16] A. Dedner, F. Kemm, D. Kröner, C.D. Munz, T. Schnitzer, M. Wesenberg, Hyperbolic divergence cleaning for the MHD equations, J. Comput. Phys. 175 (2002) 645–673.

[17] P. Degond, P.F. Peyrard, G. Russo, Ph. Villedieu, Polynomial upwind schemes for hyperbolic systems, C. R. Acad. Sci. Paris Sér. I 328 (1999) 479–483.

[18] R. Donat, A. Marquina, Capturing shock reflections: An improved flux formula, J. Comput. Phys. 125 (1996) 42–58.

[19] M. Dumbser, E.F. Toro, On universal Osher-type schemes for general nonlinear hyperbolic conservation laws, Commun. Comput. Phys. 10 (2011) 635–671.

[20] M. Dumbser, E.F. Toro, A simple extension of the Osher Riemann solver to non-conservative hyperbolic systems, J. Sci. Comput. 48 (2011) 70–88.

[21] B. Einfeldt, C.D. Munz, P.L. Roe, B. Sjögreen, On Godunov-type methods near low densities, J. Comput. Phys. 92 (1991) 273–295.

[22] J.M. Gallardo, S. Ortega, M. de la Asunción, J.M. Mantas, Two-dimensional compact third-order polynomial reconstructions. Solving nonconservative hyperbolic systems using GPUs, J. Sci. Comput. 48 (2011), 141–163.

[23] A. Harten, P.D. Lax, B. van Leer, On upstream differencing and Godunov type schemes for hyperbolic conservation laws, SIAM Rev. 25 (1983) 35–61.

[24] C. Hu, C.-W. Shu, Weighted essentially non-oscillatory schems on triangular meshes, J. Comput. Phys. 150 (1999) 97–127.

[25] G.S. Jiang, C.C. Wu, A high-order WENO finite difference scheme for the equations of ideal magnetohydrodynamics, J. Comput. Phys. 150 (1999) 561–594.

[26] F. Li, C.-W. Shu, Locally divergence-free discontinuous Galerkin methods for MHD equations, J. Sci. Comput. 22-23 (2005) 413–442.

[27] G. dal Maso, P.G. LeFloch, F. Murat, Definition and weak stability of nonconservative products, J. Math. Pures Appl. 74 (1995) 483–548.

[28] A. Marquina, Local piecewise hyperbolic reconstructions for nonlinear scalar conservation laws, SIAM J. Sci. Comput. 15 (1994) 892–915.

[29] D.J. Newman, Rational approximation to $|x|$, Michigan Math. J. 11 (1964) 11–14.

[30] S.A. Orszag, C.M. Tang, Small scale structure of two-dimensional magnetohydrodynamic turbulence, J. Fluid Mech. 90 (1979) 129–143.

[31] S. Osher, F. Solomon, Upwind difference schemes for hyperbolic conservation laws, Math. Comput. 38 (1982) 339–374.

[32] C. Parés, Numerical methods for nonconservative hyperbolic systems: a theoretical framework, SIAM J. Num. Anal. 44 (2006) 300–321.

[33] C. Parés, M.J. Castro, On the well-balance property of Roe method for nonconservative hyperbolic systems. Applications to shallow-water systems, M2AN 38 (2004) 821–852.

[34] S. Serna, A characteristic-based nonconvex entropy-fix upwind scheme for the ideal magnetohydrodynamics equations, J. Comput. Phys. 228 (2009) 4232–4247.

[35] P.L. Roe, Approximate Riemann solvers, parameter vectors, and difference schemes, J. Comput. Phys. 43 (1981) 357–372.

[36] E. F. Toro, Riemann Solvers and Numerical Methods for Fluid Dynamics, third ed., Springer, 2009.

[37] M. Torrilhon, Krylov-Riemann solver for large hyperbolic systems of conservation laws, SIAM J. Sci. Comput. 34 (2012) A2072–A2091.

[38] G. Tóth, The $\nabla \cdot \mathbf{B} = 0$ constraint in shock-capturing magnetohydrodynamics codes, J. Comput. Phys. 161 (2000) 605–652.

[39] I. Toumi, A weak formulation for Roe approximate Riemann solver, J. Comput. Phys. 102 (1992) 360–373.

[40] A.L. Zachary, A. Malagoli, P. Colella, A higher-order Godunov method for multidimensional magnetohydrodynamics, SIAM J. Sci. Comput. 15 (1994) 263–284.